



High- and low-latitude forcing of the Nile River regime during the Holocene inferred from laminated sediments of the Nile deep-sea fan

Cécile L. Blanchet ^{a,b,*}, Rik Tjallingii ^b, Martin Frank ^a, Janne Lorenzen ^a

The termination of the AHP was marked by a southward shift of the African monsoon and associated rainfall belts causing a retreat of the extensive Saharan grassland and the desiccation of vast system of lakes and rivers within the Sahara (Pachur and Kröpelin, 1987; Lézine et al., 2011). The primary forcing for this wet/arid transition is thought to be the precession-forced low latitude insolation, which gradually decreased between 8 and 4 ka BP (Rossignol-Strick, 1983). However, the rate of the paleoenvironmen-

1 9 8 7

uplands of Uganda, Rwanda and Burundi, and in particular from the outflow of Lake Victoria and Lake Albert. The Sobat, the Blue Nile and the Atbara rivers originate from the Ethiopian Highlands. Prior to the construction of the Aswan Dam (which presently traps most of the particulate matter), the sedimentation on the Nile delta was largely controlled by seasonal variations in precipitation onto the Nile watershed. The White Nile and Sobat rivers contribute a relatively continuous amount of water throughout the year given that the wet season in the Equatorial upland region lasts for more than 8 months (Fig. 1a and b) (Nicholson, 2000). The Blue Nile and Atbara tributaries contribute large amounts of water in summer when the African Rain Belt migrates to its northernmost location (Fig. 1a). Most of the sediment transported by the Nile River originates from the marked summer floods of the Blue Nile and the Atbara Rivers (Adamson et al., 1980; Williams et al., 2006). Therefore, although the White Nile is responsible for a third of the annual flow of the Nile (and up to 80% in the drier months), it provides only about 3.5% of the annual sediment load (Fig. 1c). In contrast, the Blue Nile and Atbara together supply $\sim 65\%$ of the annual flow and 96.5% of the annual sediment load (Adamson et al., 1980). The Blue Nile and Atbara also run through mantle-derived volcanic rocks that are more susceptible to erosion than the crystalline basement of the White Nile catchment.

Eolian dust is deposited on the Nile Delta at a rate of $20\text{--}40\text{ g m}^{-2}\text{ yr}^{-1}$ and mostly originates from North African sources and especially the Lybian desert (Herut et al., 2001; Prospero et al., 2002). This source is mainly active during the spring and is related to the North Atlantic Oscillation on interdecadal scale (Guerzoni et al., 1997; Moulin et al., 1997).

3. Materials and Methods

3.1. Sediment core P362/2-33

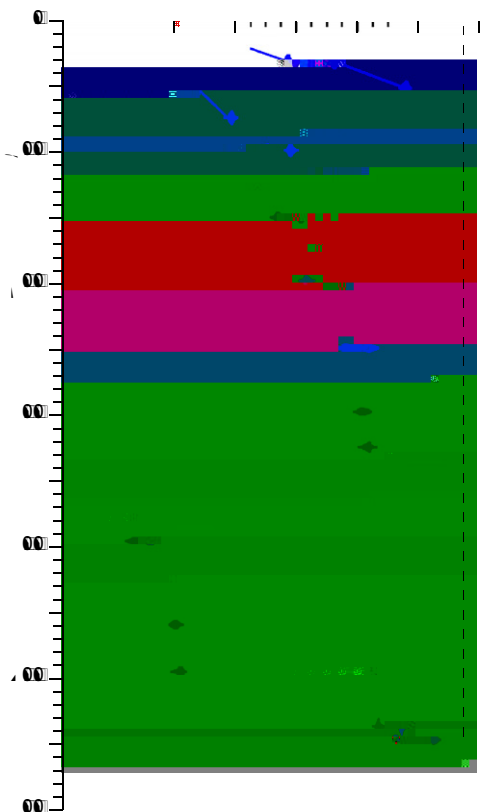
Marine sediment core P362/2-33 was recovered on the Nile deep-sea fan ($31^{\circ}40.51\text{N}$; $29^{\circ}45.00\text{E}$) during R/V Poseidon cruise P362/2 in August 2008 (Fig. 1d) (Feseker et al., 2010). This 559-cm long gravity core consists of undisturbed laminated hemi-pelagic sediments of which the upper 40 cm show a gradual change from brownish to grayish color with yellowish oxidation spots and traces of bioturbation (Fig. 4). Faint laminations are observed

(

siliciclastic fraction prior to analyzing the neodymium and strontium radioisotope signatures. The changes in proportion of the EMs were explored using log ratios in order to avoid the constant-sum constraint.

3.2.4. Radiogenic isotopes

The radiogenic isotope composition of neodymium (Nd) and strontium (Sr) was measured on the siliciclastic fraction of the sediments. Based on the results of the EMMA, the siliciclastic fraction was separated into three different grain-size fractions ($\leq 2 \mu\text{m}$, $2-10 \mu\text{m}$ and $\geq 10 \mu\text{m}$) using a centrifuge. Centrifugation time was calculated using the freeware 'Sedicalc' (Krumm, 2006). Those fractions of about 0.05 g were totally dissolved using subsequently: (i) concentrated nitric and hydrofluoric acid and (ii) concentrated nitric, hydrofluoric and perchloric acids. Standard column-chromatography procedures were applied to separate and purify Nd and Sr (Cohen et al., 1988; Horwitz et al., 1992). The Nd and Sr isotope composition was measured on a Nu Instruments multi-collector inductively-coupled plasma mass spectrometer (MC-ICP-MS) at the GEOMAR. Blank levels were



sediment composition, lithology and diagenesis (Fig. 4a–d). The MS gives an estimation of the amount of iron oxides, in particular of magnetite (Fe_3O_4) in the sediments, which originate from continental surface erosion and can be depleted during early diagenesis (Jørgensen and Kasten, 2006). The Mn/Al and Ba/Al ratios are used to identify layers of diagenetic accumulation of Mn and Ba (Reitz et al., 2006) and Ba/Al is also related to changes in export production (Mercone et al., 2000). The Mn/Al and Ba/Al ratios have been widely used to identify the extent of the sapropel layers and the occurrence of burn-down processes (De Lange et al., 2008). The downward-migration of the redox front after the sapropel deposition might indeed lead to complete removal of the TOC in the upper part of the sapropel layers, whereas Ba/Al remains unaffected (Froelich et al., 1979). In core P362/2-33, enrichments in Mn/Al and Ba/Al are observed in the upper 25 cm (at 5 and 20 cm) and are accompanied by high values in the MS (200×10^{-5} at ~ 10 cm) and in the TOC content. This probably reflects the on-going reduction of manganese and iron oxides during the microbial degradation of organic matter (Jørgensen and Kasten, 2006). The peak in Mn/Al and Ba/Al at 25 cm most likely indicates the location of the present redox front, where upward-migrating Ba^{2+} and downward-migrating Mn^{2+} did precipitate. The laminated interval is characterized by low MS values ($\leq 50 \times 10^{-5}$ SI), low Mn/Al ratios and higher TOC content

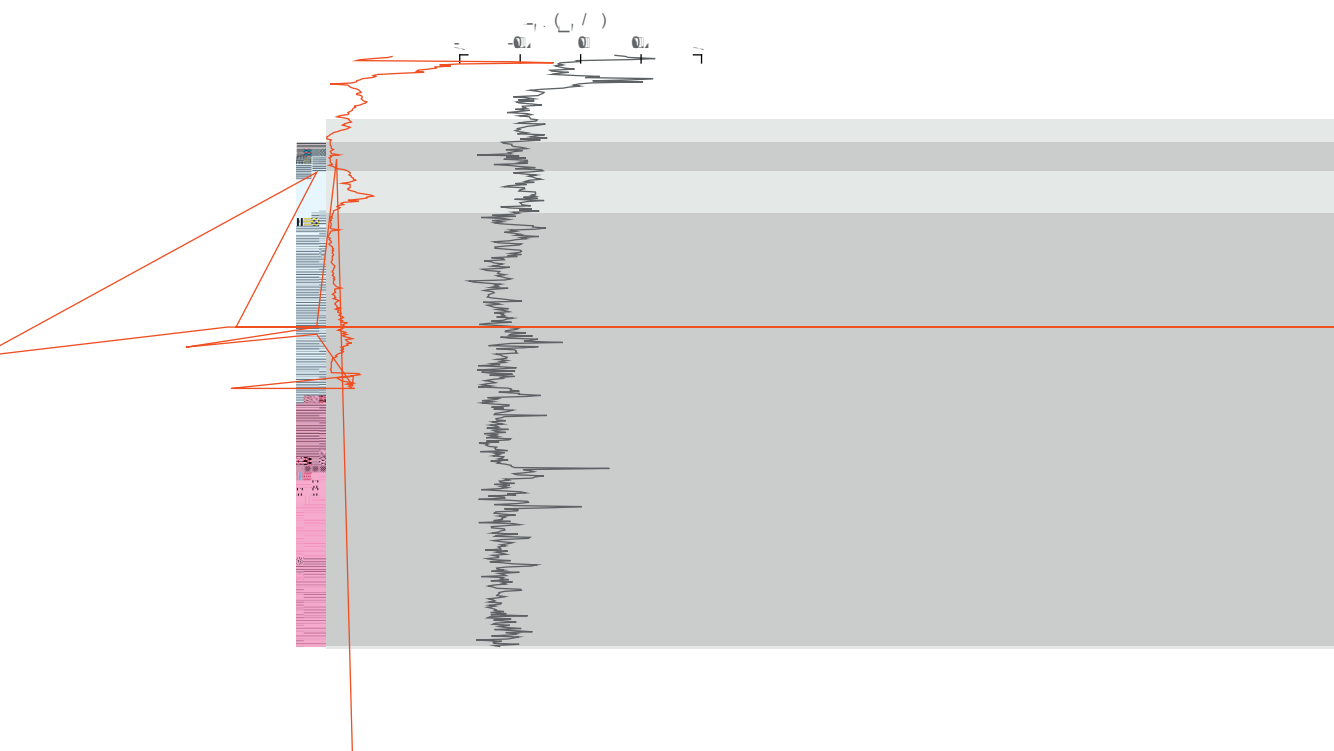
($\sim 1.1\%$). The Ba/Al ratio increases upwards throughout the laminated interval and is high between 60 and 90 cm. Both the Ba/Al ratio and the TOC content start to decrease at 80 cm (which is the last occurrence of laminations) but show a major decrease at 60 cm. This suggests that burn-down processes were of minor influence in core P362/2-33 on the TOC content and that the sapropel layer extends up to 60 cm. The absence of extensive burn-down processes was already observed for cores with high accumulation rates in this region (Mercone et al., 2000).

The changes in marine/terrestrial material and within the detrital material are investigated by comparing the Ti/Ca and Ti/Al ratios (Fig. 4e and f). These ratios show a relatively similar pattern, with higher values in the sapropel layer, lower values between 40 and 20 cm and high values in the upper 10 cm. The enrichment of the sapropelic sediments in Ti most probably indicates a higher contribution by Nile particulate matter (Krom et al., 1999). The Ti/Ca and Ti/Al ratios decrease gradually between 100 and 25 cm, which suggest a progressive reduction of river input.

5.2. Grain-size distribution: sources and transportation mechanisms of terrigenous particles

Terrigenous particles deposited in marine sediments generally originate from distinct sources and underwent different modes of transport, which are characterized by specific grain-size distributions (Weltje and Prins, 2003). For our dataset, a three end-member (EM) model explained about 99.5% of the total variance and allowed the definition of a coarse multimodal EM (EM1) and two bimodal hemipelagic EMs (EM2 and EM3) (Fig. 3d). The poorly sorted grain-size distribution of EM1 ranges from 0.1 to 200 μm with two main modes between 15 and 30 μm . The grain-size distributions of the two hemipelagic EM2 and EM3 range between 0.1 and ~ 40 μm , with distinct modal grain-sizes of 3–4 μm and 2 μm , respectively. The grain-size distribution of the EMs matches that of present-day fluvial and eolian material collected in the region. Like the EM1, the grain-size distributions of Mediterranean aerosols range from 1 to 100 μm and are typically poorly sorted with a modal size of 10–30 μm (Guerzoni et al., 1997). Like the hemipelagic EM2 and EM3, the Nile River particles fall into the mud size-fraction, with particles originating from the Blue Nile being generally coarser than those originating from the White Nile (Billi and el Badri Ali, 2010). Coarser particles are indeed produced by the intense erosion occurring during summer floods in the erodible volcanic watershed of the Blue Nile. In contrast, the year-round precipitation pattern at the source of the White Nile enables the development of a vegetation cover that tends to protect the more resistant crystalline basement from erosion. Furthermore, the sediment load of the White Nile is filtered when passing into the large swamps of the Sudd, before the convergence with the Blue Nile and Atbara Rivers (Williams et al., 2006). These climatic, geographic and geologic differences also explain that most sediment presently delivered to the margin originates from the Blue Nile drainage area (Adamson et al., 1980). Therefore, we assume that EM2 is enriched in coarser particles originating from floods of the Blue Nile River as compared to EM3.

In order to further assess the provenance of the EMs, we separated four samples into three grain-size fractions (≤ 2 μm , 2–10 μm and ≥ 10 μm) and measured their Nd and Sr radioisotope composition (Table 2 and Figs. 5 and 6). The samples collected at 30, 85 and 221 cm depth contain dominant proportions of EM1, EM3 and EM2, respectively (Fig. 5). The sample collected at the core-top (0 cm depth) contains an equal proportion of EM2 and EM3. The EM2 and EM3 have ϵNd values that are not significantly different and comprised between ~ 0 and



from the White Nile between 8 and 6 ka was also hypothesized from Eastern Mediterranean sediment cores (Revel et al., 2010; Box et al., 2011). The Late Holocene increase in Blue Nile contribution was observed using Sr isotopic signature of sediments from the eastern Nile Delta (Krom et al., 2002) (Fig. 7e).

6. Conclusions

6.1. Influence of low-latitude insolation

The changes in fluvial discharge and source areas as recorded by core P362/2-33 have apparently been primarily controlled by summer and spring/autumn low-latitude insolation changes. The river runoff gradually decreased between 8 and 4 ka BP (Fig. 8b and c) following the summer insolation at 20°N (Fig. 8a). Precession-forced insolation changes at low latitudes are the principal control on the position and strength of monsoonal systems and related precipitation belts (Gasse, 2000; Haug et al., 2001; Wang et al., 2001; Tjallingii et al., 2008). We therefore postulate that the total runoff of the Nile has mainly been controlled by changes in precipitation within the overall drainage area, which was related to a contraction of the African Rain Belt around the Equator following the changes in summer insolation after 10 ka BP (Gasse, 2000; Collins et al., 2011).

The changes in relative intensity of the Blue Nile discharge have mainly been driven by variations in spring/autumn low-latitude insolation (Fig. 8e and f). Sediment supply by the Blue Nile was enhanced during the early and late Holocene at times of higher spring insolation, and was reduced between 8 and 4 ka at times of low spring insolation and high autumn insolation (Fig. 8e and f). Additionally, periods of enhanced supply from the Blue Nile positively correlate with high sedimentation rates during the early Holocene, but this is not observed during the late Holocene

of coarse sediments originating from the Blue Nile between 8.5 and 7.3 ka BP as indicated by the decrease in EM2/EM3 ratio (Fig. 7e) is synchronous with a rapid decrease in sedimentation rate (Fig. 7f). The Blue Nile was obviously the principal contributor of fluvial sediments from 9.5 to 8.5 ka BP, after which its influence decreased abruptly to reach a minimum at 7.3 ka BP. The relative contribution from the Blue Nile remained low until ~6 ka BP while the relative contribution from White Nile was perhaps enhanced. Interestingly, the increase in proportion of material from the Blue Nile between 3 and 1 ka BP was not accompanied by an increase in sedimentation rate. These observations suggest that switches in the fluvial source areas controlled the sedimentation supply only during periods of high fluvial input, such as the AHP. Our reconstructed changes in relative intensity of the Blue Nile discharge to the Nile deep-sea fan agree with previous studies. Higher Blue Nile sediment flux during the early and late Holocene was estimated from marine sediments from the Levantine Basin based on their Sr isotopic signature (Box et al., 2011) (Fig. 7d). Enhanced supply of material



(Fig. 8f and g). These changes are best explained by shifts in the seasonal distribution of insolation following the precession of the equinoxes during the Holocene (Fig. 8d) (Marzin and Braconnot, 2009).

Presently, most of the Blue Nile runoff occurs during summer and accounts for $\sim 50\%$ of the annual Nile runoff, whereas the White Nile runoff is higher during the autumn and accounts for $\sim 30\%$ of the annual Nile runoff (Fig. 1) (Williams et al., 2006). In addition, most of the sediment load of the Nile today is provided by the Blue Nile ($\sim 70\%$), whereas the contribution of the White Nile is negligible ($\sim 4\%$). This predominance of supply by the Blue Nile is largely related to the current orbital configuration, with the peak of insolation occurring during the boreal summer solstice (Fig. 8d). During the early Holocene the peak of insolation also occurred during the summer solstice but the summer insolation in the northern Hemisphere tropics was enhanced by $\sim 10\%$ compared to today (Fig. 8a). Higher summer insolation most likely enhanced the precipitation in the source area of the Blue Nile and lead to higher runoff and erosion in the Blue Nile watershed (Fig. 8g). Elevated lake levels were observed at the source of the Blue Nile during the early Holocene and were also related to an increased summer insolation (Gasse, 2000; Marshall et al., 2011; Garcin et al., 2012). At 6 ka BP, summer insolation in the North Hemisphere tropics was also higher relative to today (by $\sim 6\%$) but was shifted toward the autumn equinox. We speculate that the decrease in summer insolation and the increase in autumn insolation led to a decrease in relative intensity of the Blue Nile discharge and perhaps to a relative increase in White Nile runoff (which occurs today mostly in autumn). Changes in lake levels in the African equatorial band have been related to changes in summer and spring insolation before (Garcin et al.,

2009; Verschuren et al., 2009) and Lake Victoria, which is located at the source of the White Nile, had a high stand between 7.8 and 5.8 ka BP (Stager et al., 2003

large-scale hydrological perturbation occurred in equatorial and tropical Africa around 8.5 ka BP, which was characterized by low-stands in most lake records from northern Africa (Gasse, 2000).

occurrence of the North African event, which has consistently been dated between 8.6 and 8.4 ka BP, led other authors to propose that the large hydrological change in low latitudes was a potential trigger for the 8.2 ka cooling event (Shanahan et al., 2007; Marshall et al., 2011). Our record shows a disruption of the AHP at 8.5 ka but does not provide any further support in favor of any of these scenarios.

Another remarkable climatic event of our record is the highly arid period between 4.3 and 3.7 ka BP, which represents a culmination in the gradual development of arid conditions in the drainage area of the Nile River. This event was characterized by a marked increase in dust contribution and by a slight decrease in relative intensity of the Blue Nile discharge (Fig. 8b, c and f). Many terrestrial records in North Africa depict the existence of a short-lived arid period centered at ~ 4 ka BP, such as indicated by low lake levels (e.g., Gasse, 2000), enhanced dust deposition in Kilimanjaro ice cores and in the Gulf of Oman (Cullen et al., 2000; Thompson et al., 2002) and the cessation of runoff in the Wadi Howar river system, which was a major tributary of the Nile River during the AHP (Pachur and Kröpelin, 1987). A growing number of studies have reported a short period of intense drought occurring as the apex of a gradual aridification. For instance, the decrease in runoff to the Lake Tana Basin (Marshall et al., 2011), the development of aridification on the Somalian coast (Jung et al., 2004) and the vegetation transition at Lake Yoa (Kröpelin et al., 2008) all took place between 6.5 and 4.2 ka BP. The mechanisms underlying this drought event are highly complex and may involve meridional teleconnection such as those discussed for the 8.2 ka event (deMenocal et al., 2000b; Wang et al., 2004). In addition, threshold responses of environmental systems (e.g., lake overflows) may have been responsible for the abruptness of changes in some climatic records. This drought event has been proposed to represent the actual end of the AHP (Marshall et al., 2011).

It is noted that both events were so severe that they had a large impact on population dynamics in northern Africa as illustrated by the changes in phases of human settlements reconstructed by Kuper and Kröpelin (2006). The drought event at 4.2 ka BP was also linked with the end of the Akkadian society in Mesopotamia and of the Old Kingdom in Egypt, which have both been dated at 4.17 ka BP (Cullen et al., 2000; Stanley et al., 2003).

6.2. Influence of changes in the Nile River regime on the bottom-water oxygenation

Millimeter-scale laminations prevail in core P362/2-33 for the period between 9.5 and 7.3 ka BP (Fig. 8). The lithology of this part of the core is similar to laminated sediments described in another sediment core from the Nile deep-sea fan, which were interpreted as hyperpycnal flows forming during seasonal Nile floods (see Section 3.1) (Ducassou et al., 2008). The preservation of these seasonal laminations implies that bioturbation was prevented due to very high sedimentation rates and low bottom-water oxygen levels (Rossignol-Strick et al., 1982; Ducassou et al., 2008). The O₂-depletion occurred throughout the Mediterranean Basin and has been related to the large influx of fresh water and nutrients from the Nile River, which essentially shut down the Mediterranean thermohaline circulation and enhanced primaryu53ic.3ic3b16(d)-menta36.2-243.784.9(im)im8.4(a14.3(m0(n)16(d)-802.3(en)16(h4.3uee3088.

supervised the grain-size measurements. Great help was also provided by our colleagues at the GEOMAR for the radioisotope measurements and discussions with Lukas Jonkers helped improving the manuscript.

References

- Adamson, D.A., Gasse, F., Street, F.A., Williams, M.A.J., 1980. Late Quaternary history of the Nile. *Nature* 288, 50–55.
- Alley, R.B., Mayewski, P.A., Sowers, T., Stuiver, M., Taylor, K.C., Clark, P.U., 1997. Holocene climatic instability: a prominent, widespread event 8200 yr ago. *Geology* 25, 483–486.
- Billi, P., el Badri Ali, O., 2010. Sediment transport of the Blue Nile at Khartoum. *Quat. Int.* 226, 12–22.
- Blaauw, M., Christen, J., 2011. Flexible paleoclimate age-depth models using an autoregressive gamma process. *Bayesian Anal.* 6, 457–474.
- Box, M., Krom, M., Cliff, R., Bar-Matthews, M., Almogi-Labin, A., Ayalon, A., Paterne, M., 2011. Response of the Nile and its catchment to millennial-scale climatic change since the LGM from Sr isotopes and major elements of East Mediterranean sediments. *Quat. Sci. Rev.* 30, 431–442.
- Brovkin, V., Bendsten, J., Claussen, M., Ganopolski, A., Kubatzki, C., Petoukhov, V., Andreev, A., 2002. Carbon cycle, vegetation, and climate dynamics in the Holocene: experiments with the CLIMBER-2 model. *Global Biogeochem. Cycles* 16.
- Claussen, M., Kubatzki, C., Brovkin, V., Ganopolski, A., Hoelzmann, P., Pachur, H.J., 1999. Simulation of an abrupt change in Saharan vegetation in the mid-Holocene. *Geophys. Res. Lett.* 26, 2037–2040.
- Cohen, R.K., O’Nions, A.S., Siegenthaler, R., Griffin, W.L., 1988. Chronology of the pressure–temperature history recorded by a granulite terrain. *Contrib. Mineral. Petrol.* 98, 303–311.
- Collins, J.A., Schefuß, E., Heslop, D., Mulitza, S., Prange, M., Zabel, M., Tjallingii, R., Dokken, T.M., Huang, E., Mackensen, A., Schulz, M., Tian, J., Zariwaei, M., Wefer, G., 2011. Interhemispheric symmetry of the tropical African rainbelt over the past

